Improvement of Depth Position in 2-D/3-D Registration of Knee Implants Using Single-Plane Fluoroscopy

Takaharu Yamazaki*, Tetsu Watanabe, Yoshikazu Nakajima, Kazuomi Sugamoto, Tetsuya Tomita, Hideki Yoshikawa, and Shinichi Tamura

***Abstract*—Two-dimensional (2-D)/three-dimensional (3-D) registration techniques using single-plane fluoroscopy are highly important for analyzing 3-D kinematics in applications such as total knee arthroplasty (TKA) implants. The accuracy of single-plane fluoroscopy-based techniques in the determination of translation perpendicular to the image plane (depth position), however, is relatively poor because a change in the depth position causes only small changes in the 2-D silhouette. Accuracies achieved in depth position using conventional 2-D/3-D registration techniques are insufficient for clinical applications. Therefore, we propose a technique for improving the accuracy of depth position determination in order to develop a system for analyzing knee kinematics over the full six degrees of freedom (6 DOF) using single-plane fluoroscopy. In preliminary experiments, the behaviors of errors for each free variable were quantified as evaluation curves by examining changes in cost function with variations in the free variable. The evaluation curve for depth position was more jagged, and the curve peak less pointy, compared to the evaluation curves of the other five variables, and the curve was found to behave differently. Depth position is therefore optimized independently of the other variables, using an approximate evaluation curve of depth position prepared after initial registration. Accuracy of the proposed technique was evaluated by computer simulation and *in vitro* tests, with validation of absolute position and orientation performed for each knee component. In computer simulation tests, root-mean-square error (RMSE) in depth position was improved from 2.6 mm (conventional) to 0.9 mm (proposed), whereas for *in vitro* tests, RMSE improved from 3.2 mm to 1.4 mm. Accuracy of the estimation of the remaining two translational and three rotational variables was found to be almost the same as that obtained by conventional techniques. Results of *in vivo* tests are also described in which the possibility of full 6 DOF kinematic analysis of TKA implants is shown.**

***Index Terms*—Depth position, evaluation curves, independent optimization, kinematics, single-plane fluoroscopy, 2-D/3-D registration.**

Manuscript received August 30, 2003; revised January 26, 2004. The Associate Editor responsible for coordinating the review of this paper and recommending its publication was W. J. Niessen. *Asterisk indicates corresponding author.*

*T. Yamazaki is with the Division of Interdisciplinary Image Analysis, Department of Medical Robotics and Image Sciences, Osaka University Graduate School of Medicine, 2-2 Yamadaoka, Suita, Osaka 565-0871, Japan (e-mail: yamazaki@image.med.osaka-u.ac.jp).

T. Watanabe and K. Sugamoto are with the Division of Computer Integrated Orthopaedic Surgery, Department of Medical Robotics and Image Sciences, Osaka University Graduate School of Medicine, Osaka 565-0871, Japan.

Y. Nakajima and S. Tamura are with the Division of Interdisciplinary Image Analysis, Department of Medical Robotics and Image Sciences, Osaka University Graduate School of Medicine, Osaka 565-0871, Japan.

T. Tomita and H. Yoshikawa are with the Department of Orthopaedics, Osaka University Graduate School of Medicine, Osaka 565-0871, Japan.

Digital Object Identifier 10.1109/TMI.2004.826051

I. Introduction

In orthopedics, quantitative assessment of the three-dimensional (3-D) dynamic motion of skeletal joints under *in vivo* conditions allows objective evaluation of joint diseases and dysfunctions and is very important in the establishment of next-generation diagnosis and therapy techniques. Particularly in the field of adult knee surgery, kinematic analyses of total knee arthroplasty (TKA) have clarified several *in vivo* motions of knee implants and have attracted attention in recent years [1], [2]. At present, knee implants designed for long-life durability and high activity are available, and in order to identify the optimal design of knee implants, it is necessary to accurately quantify the 3-D motion of the implants under *in vivo* conditions.

In recent years, 3-D pose estimation [two-dimensional (2-D)/3-D registration] techniques, in which an X-ray fluoroscopy system is used to estimate the position and orientation of an object based on projected 2-D images, have been developed [3]–[9] and applied to 3-D kinematic analyses and computer aided surgery. The basic principle of these techniques is that a 3-D object with a known shape and size is matched to a projected 2-D image in order to determine the six degrees of freedom (6 DOF), or the position and orientation, of the object. Several techniques [3]–[6] have been proposed for 2-D/3-D registration of TKA implants by single-plane fluoroscopy. These techniques are highly valuable for dynamic 3-D kinematic analyses. However, although clinically sufficient accuracy has been obtained for the five degrees of freedom (5 DOF) of two translations parallel to fluoroscopic images and three rotations, sufficient accuracy has not been obtained for the one degree of freedom (1 DOF) of translation perpendicular to fluoroscopic images (depth position). In clinical applications, the accuracy of the depth position should ideally be about 1 mm, while some researchers report that absolute errors of 2–10 mm have been obtained by computer simulation tests. In order to address this problem, conventional techniques assumed that there is no displacement between the femoral and tibial components on lateral images of the knee. In other words, depth position was ignored, and relative medio-lateral translation was set to zero. However, there is a variety of knee implant designs, for example, implants having a low coronal constraint or those without a posterior stabilizer, thus medio-lateral shift of the knee may be induced by daily living activities. In recent years, medio-lateral shift caused by femoral condylar lift-off has also been reported [10]. Thus, with the conventional techniques, the accuracy of analysis with regard to medio-lateral translation is insufficient. As a result, knee implant kinematics can analyze the 5 DOF, but not the depth position.

As for techniques that can measure the 6 DOF of a 3-D object, including depth position, with a sufficient level of estimation accuracy, 2-D/3-D registration techniques utilizing biplane fluoroscopy have been reported [11]. However, with biplane fluoroscopy, a sufficient amount of space for testing cannot be ensured for human joints undergoing dynamic motion. Therefore, biplane fluoroscopy can be used mostly for computer aided surgery or static joint kinematic analysis. Problems such as limited space for testing, system complexity and increased radiation exposure remain unresolved.

With any 2-D/3-D registration technique using single-plane fluoroscopy, the accuracy of depth position is less than that for the other 5 DOF because the distance between the X-ray focus and the object is large, and as a result, the amount of information for changes in the projected 2-D silhouette is smaller than that for depth changes. The much smaller effect of depth variable has been described by a previous study [9], and these errors have also been quantified [3]–[6], [9]. In our study, for the purpose of improving the accuracy of depth position, we quantified the behaviors of errors for each free variable as evaluation curves, and then analyzed the resulting evaluation curves. The results showed that when compared to the other 5 DOF, the evaluation curve for depth position was more jagged and the curve peak less pointy. Therefore, we propose a technique in which depth position is optimized based on its evaluation curve independently of the other 5 DOF: Estimation of all 6 DOF of a knee implant is thus accomplished by determining the 3-D pose of a model through simultaneous optimization based on the nonlinear least-square method, which is used for the conventional 2-D/3-D registration technique, and then utilizing our proposed depth position improvement technique. We also apply this proposed technique to dynamic kinematic analyses of knee implants under *in vivo* conditions.

In this paper, Section II details the materials and methods for developing a full 6 DOF kinematic analysis system for knee implants using single-plane fluoroscopy; Section II-D details the technique for improving the accuracy of depth position; Section III-A describes the preliminary experiments, including the evaluation curve preparation; Section III-B describes the experimental methods for computer simulation, *in vitro* and *in vivo* tests, and the results of a comparison between proposed and conventional techniques; and Section IV discusses the study results.

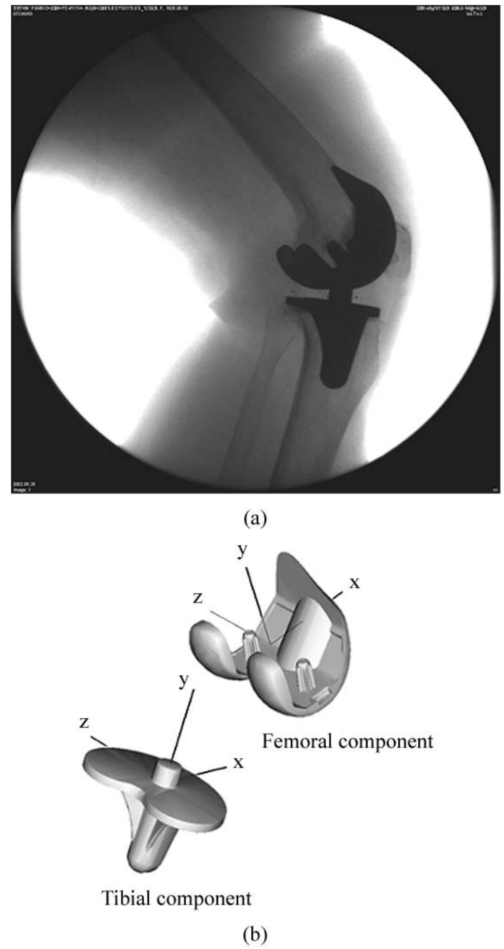

Fig. 1. (a) X-ray fluoroscopic image of knee prosthesis (femoral and tibial components) under *in vivo* conditions. (b) Femoral and tibial implant CAD models used knee prosthesis design. Relevant prosthesis coordinate systems are shown.

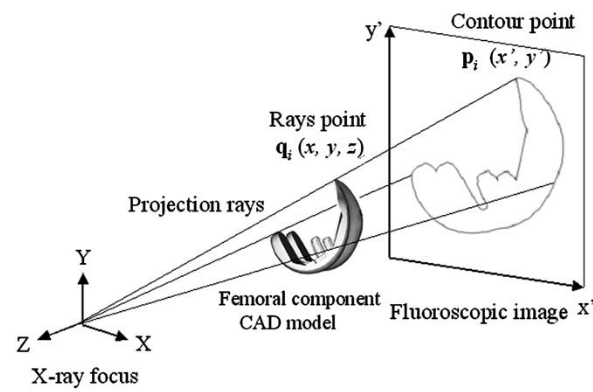

Fig. 2. Perspective projection model of single-plane fluoroscopy.

II. Materials and Methods

A. Overview

To achieve 2-D/3-D registration of a knee implant using single-plane fluoroscopy, it is necessary to have an accurate structural model of the knee implant and to know the parameters of the imaging system. The 3-D geometry of the knee implant was taken from computer assisted design (CAD) data of the implant. Parameters of the imaging system were determined using a perspective projection model of X-ray fluoroscopy. In fluoroscopy, X-rays are emitted from a point source, pass through the knee and are then incident upon an image intensifier (II). A visible image is produced by the II and recorded by a charge-coupled device (CCD) camera. The silhouette of the knee implant obtained is a perspective projection, which is slightly distorted by curvature of the II screen. True perspective projections are obtained by performing distortion correction on the raw fluoroscopic image. Fig. 1(a) and (b) shows uncorrected X-ray fluoroscopic images of knee implants (femoral and tibial components) and CAD models of two different knee implants. Fig. 2 illustrates the perspective projection model in single-plane fluoroscopy. In this paper, the pose estimation of a knee implant is built on contour-based 2-D/3-D registration because metallic knee implants appear much darker than the surrounding soft tissue [Fig. 1(a)] and the edge detection is a relatively easy image processing task. To improve the accuracy of depth position, the evaluation curve, which gives a quantitative indication of estimation errors, is prepared and used to optimize depth estimation. The presented technique is based on the idea that the accuracy of depth position can be improved by optimizing it using its evaluation curve independently of the other 5 DOF, after making an initial estimation.

B. Determination of Imaging System Parameters

To determine parameters of the imaging system, the position of the X-ray focus with respect to the image plane needs to be calibrated. First, a 217-marker 3-D calibration board is placed in the viewing area of the imaging system and X-ray images are acquired. Second, the X-ray image is corrected using a nonlinear distortion correction technique [12] to retrieve true perspective projection images. Finally, intrinsic parameters (principal point and principal distance) of the imaging system are determined from 2-D data (position of the center of projected markers) on the corrected X-ray images and the known 3-D data (position and orientation) of the calibration board using the calibration algorithm proposed by Weng [13]. The principal point is the point on the image plane where X-rays are incident perpendicularly, and the principal distance is the distance from the X-ray focus to the principal point.

C. Image Acquisition and Processing

The single-plane fluoroscopy system used consists of a 150-kV X-ray generator (Shimadzu model XUD150B-30; 0.6-mm nominal focal spot size), 30-cm II (Shimadzu model IA-12LT/HG), and a digital CCD camera (Shimadzu model DIGITEX PRO, $1024 \times 1024 \times 12$-bit pixels, 7.5 frames/s, progressive scan). Fluoroscopic images were not recorded onto videotape, but were recorded as a series of digital images. Tests were typically performed with the X-ray parameters of 70 kV, 400 mA, and 1.2- to 2.0-ms duration, enabling nearly blur-free imaging of motion with higher per-frame exposure and image quality than in standard video-fluoroscopy (nonpulsed, 30 frames/s).

In the image processing, a variety of edge filters have been applied to knee implant images [14], [15]. In our study, a Gaussian-Laplacian filter and threshold is applied to extract knee implant contours from distortion corrected images. However, complete contours are not necessarily detected because of the effects of other materials (bone and bone-cement) close to the knee implant, overlap of femoral and tibial components, and parts of the knee implant silhouette being outside of the field of view. Spurious edges and noise from the edge-detection process are erased manually.

D. Two–Dimensional/Three-Dimensional Registration Technique

Estimation of all 6 DOF of a 3-D object model consists of the following two steps.

Step 1) Initial 3-D pose estimation using conventional 2-D/3-D registration.

Step 2) Refinement of depth position from the extremum of the evaluation curve of depth position.

By performing independent optimization of depth position [Step 2)] on top of multivariate optimization of the six free variables [Step 1)], a 3-D pose estimation is achieved more accurately.

1) Conventional 2-D/3-D Registration: The 2-D/3-D registration technique used is built on the contour-based registration algorithm proposed by Zuffi *et al.* [6]. The algorithm is a simplified version of the algorithm originally proposed by Lavalee and Szeliski [16], and includes features that can handle occlusions, and is therefore not limited to complete contours of knee implants. The basic principle of the algorithm is that the 3-D pose of a model can be determined by projecting rays from contour points in an image back to the X-ray focus and noting that all of these rays are tangential to the model surface. Hence, a cost function E is defined as the sum of Euclidean distances d_i between all projected rays and the model surface

$$E = \sum_{i=0}^{N} d_i^2. \tag{1}$$

The Euclidean distance d_i between the point $\mathbf{s}_i$ on the model surface and point $\mathbf{q}_i$ on a ray projected from contour point $\mathbf{p}_i$ (see Fig. 2) is given by

$$d_i = \pm|\mathbf{q}_i - \mathbf{s}_i| \tag{2}$$

where $0 \leq i < N$ and N is the number of contour points. In addition, negative values indicate rays that cross the model surface. To reduce the time spent computing distances between projected rays and the model surface, a 3-D distance map of the model is pre-computed and used for these distance calculations [17]. The map stores the Euclidean distance from any point in the neighborhood of the object to the closest point on the model surface. In this study, a 3-D distance map of resolution 0.25 mm was used. The resolution is close to that of fluoroscopic images and is twice as high as that used by Zuffi *et al.* [6].

The 3-D pose is estimated by minimizing the cost function E iteratively over the 6 DOF using a nonlinear multivariate optimization technique, the Levenberg–Marquardt nonlinear least-square method [18]. A good function for determining convergence of the 3-D pose of the model is given by root-mean-square distance (RMSD)

$$\mathrm{RMSD} = \sqrt{E/N}. \tag{3}$$

Using these techniques, an initial estimation of the 3-D pose of the model is made.

2) Improvement of Depth Position: To determine depth position more accurately, the application of a technique based on polynomial curve fitting to the evaluation curve of depth position is presented.

Fig. 4 shows evaluation curves plotting RMSD against errors of each free variable (see Section III-A). It is apparent that the gradient of the evaluation curve of depth position is much lower than those of the other 5 DOF (the methods for preparing evaluation curves and the differences between them are detailed in Sections III-A1 and III-A2). Because of the significantly different behavior of depth position to the other 5 DOF, optimization of this variable is conducted independently. Furthermore,

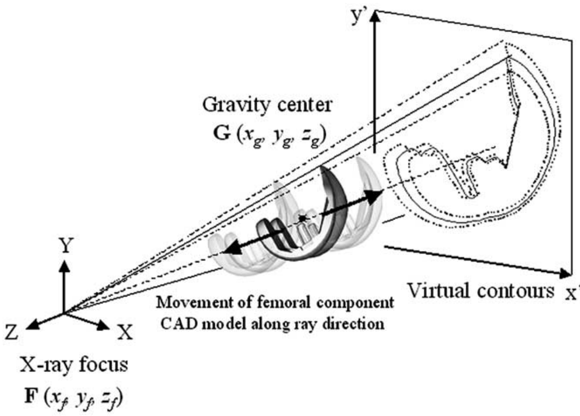

Fig. 3. Preparation of evaluation curve for depth position. After initial pose estimation, the model is moved with arbitrary step width along a straight line which connects X-ray focus $\mathbf{F}(x_f, y_f, z_f)$ and the gravity center of the model $\mathbf{G}(x_g, y_g, z_g)$, and then the change in depth position and RMSD at each step are computed.

the evaluation curve is assumed to be approximated well by a polynomial for small deviations from the global minimum because the curve for depth position was observed to be non-linear, unlike that for the other 5 DOF. Therefore, the global minimum of depth position is determined from the extremum of a polynomial (the reasonable order of polynomial is addressed in Section III-A3).

For independent optimization of depth position, after initial registration estimation, the model is moved along a straight line joining the X-ray focus $\mathbf{F}(x_f, y_f, z_f)$ to the center of gravity of the model $\mathbf{G}(x_g, y_g, z_g)$ over an arbitrary step width. RMSD is then computed at each step along the line. Fig. 3 shows movement of the model along this line and virtual silhouette contours at each of these positions. A set of points that were obtained in this way is fitted to the polynomial function given by

$$f(\Delta z) = a_0 + a_1(\Delta z) + a_2(\Delta z)^2 + \ldots + a_n(\Delta z)^n \quad (4)$$

where Δz and $f(\Delta z)$ indicate the change in depth position from $\mathbf{G}(x_g, y_g, z_g)$ at each step and the RMSD computed at each position, respectively. In addition, n is the order of the polynomial and a_{n} is an unknown parameter of the coefficients of the polynomial.

The coefficients of the polynomial are estimated by calculating the inverse function of (4) using the set of points that has already been obtained. The extremum of the resulting polynomial is calculated by solving the first derivative of the polynomial using the Durand-Kerner method [19], and the minimum extremum is selected. The minimum value is taken as the global minimum of depth position. A final estimate of all 6 DOF of the 3-D model is thus determined. In our study, in order to confirm sufficient convergence to the global minimum by refinement of depth position, conventional 2-D/3-D registration was carried out a second time using the corrected depth position.

III. Experiments

A. Preliminary Experiments

1) Evaluation Curve Preparation and Usage: In order to quantitatively analyze the behaviors of the errors for each free variable, each evaluation curve was prepared. In the computer simulation, from a known 3-D pose with a distance of 850 mm between the X-ray focus and the implant CAD model, an error was given with a slight step for each variable of translation and rotation, and the RMSD [see (3)] was then calculated. Fig. 4 shows RMSD evaluation curves by the femoral component. Besides the given error, each curve includes the error of the resolution of the image and a distance map.

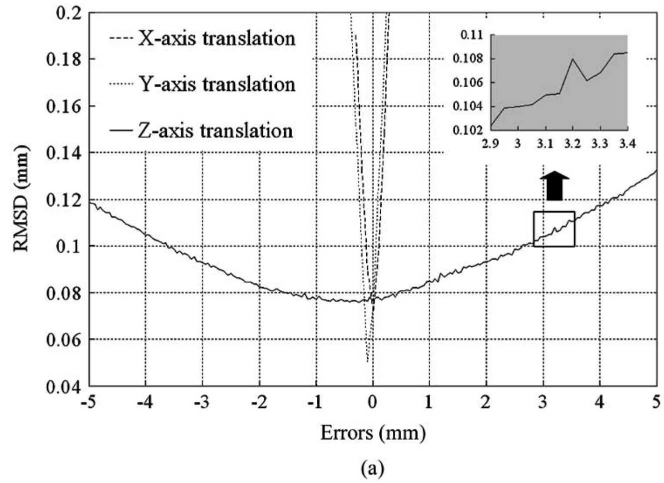

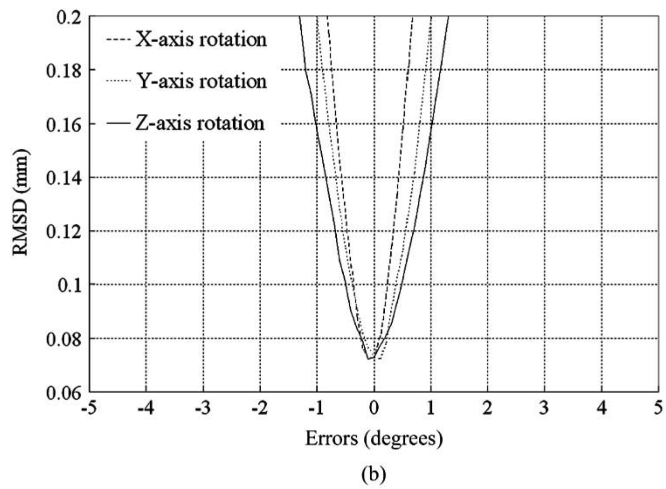

Fig. 4. Evaluation curves plotting RMSD against errors of each variable. (a) Translations. (b) Rotations. The evaluation curve for Z axis translation (depth position) is more jagged, and the curve peak less pointy, compared to the other five DOF.

Based on these results, the evaluation curve for depth position was more jagged, and the curve peak less pointy, compared to the evaluation curves of the other 5 DOF. If optimization for depth position is simultaneously performed with the other 5 DOF, the solution to the global minimum is difficult to locate and is likely to be trapped in a local minimum due to the influence of interdependency and jag. Therefore, the accuracy of depth position can be improved by optimizing it using its evaluation curve separately from the other variables. A similar analysis was performed for the tibial component, which showed similar trends as observed for the femoral component.

2) Differences in Evaluation Curves for Each Variable: Under actual clinical conditions, depth position of a knee implant can change with position for the left and right knee and standing position of the knees during dynamic motion. In

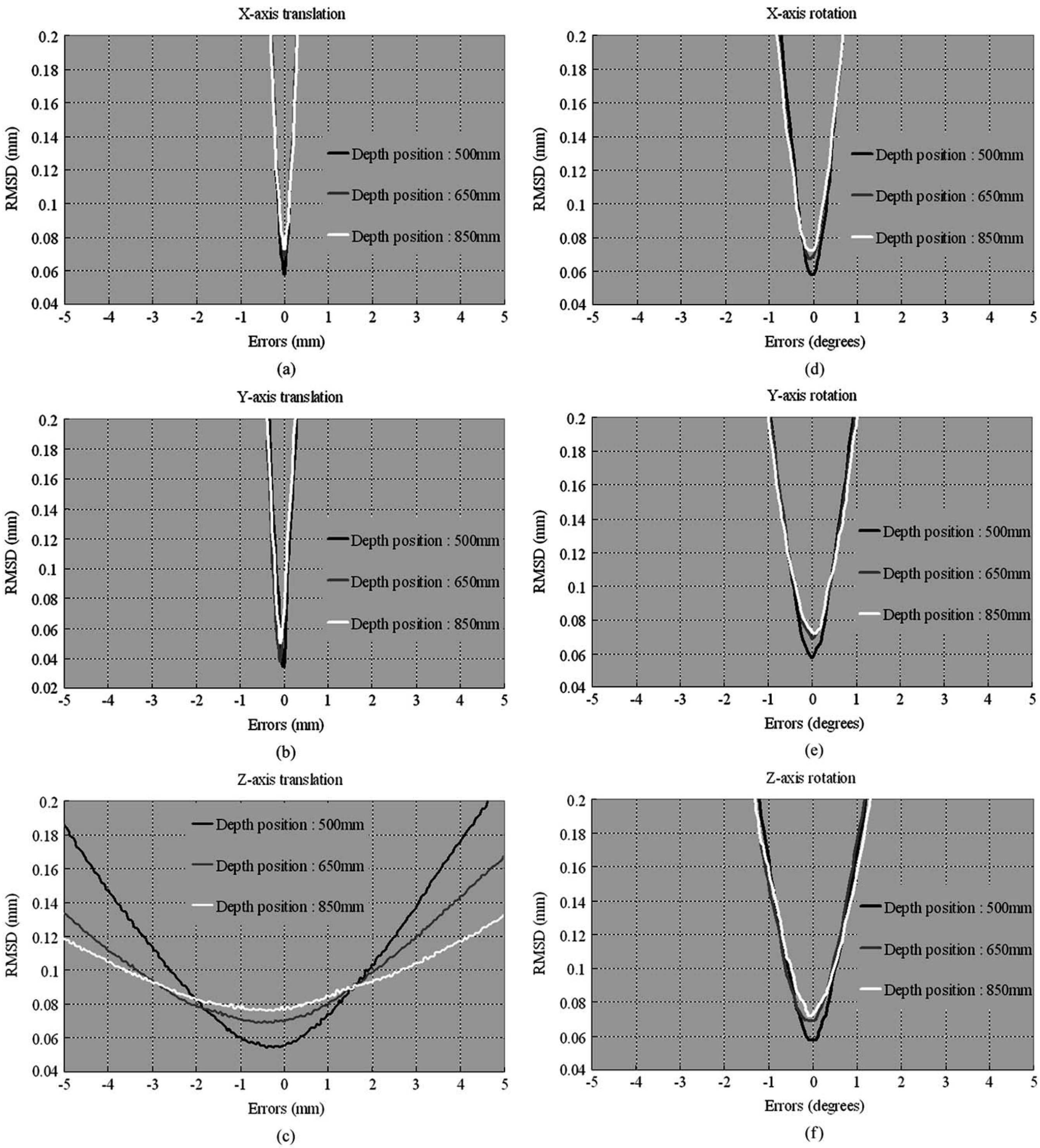

Fig. 5. Evaluation curves for each variable with 500, 650, or 850 mm between X-ray focus and the model. (a)–(c) Translations. (d)–(f) Rotations. The gradient of the evaluation curve for Z axis translation (depth position) is not only much lower than that for the other five DOF but also changes much more markedly with distance.

order to verify the influence of the variation in depth position on the evaluation curve, each evaluation curve was prepared and compared by varying the distance between the X-ray focus and the model. Fig. 5 shows the results obtained for the femoral component with a distance of 500, 650, or 850 mm.

The gradient of the curve for depth position was not only much lower than that for the other 5 DOF but also changed much more markedly with distance. Although a weighted optimization is generally applied to compensate for the difference of variable scale, it would be difficult to determine a fixed weight value for the depth position with respect to the other 5 DOF because of the difference in gradient for each evaluation curve as shown in Fig. 5(c). Our proposed technique does not require adjustment of the weight value as it uses an approximate eval-

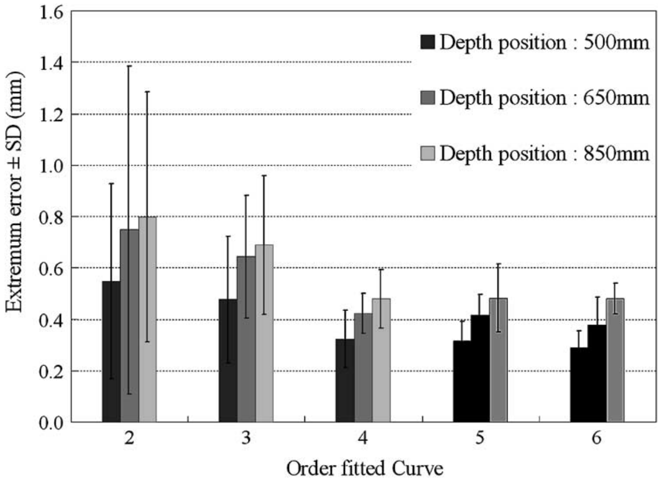

Fig. 6. Absolute distance between the extremum of each polynomial and actual depth position (extremum error), and its standard deviation (SD). Curve fitting was performed with 500, 650, or 850 mm between X-ray focus and the model.

uation curve for depth position. In other words, the increase of depth errors by insufficient scaling is removed, and as a result, a stabilized global minimum is obtained even under actual clinical conditions, as described above.

3) Determination of Order of Polynomial Curve Fitting: The evaluation curve for depth position is approximately described as a polynomial in (4). In order to obtain the extremum of a polynomial in a stable and simple manner, a reasonable order of a polynomial was experimentally investigated. In our study, ten different points of depth position given over ± 1 mm steps and each resulting RMSD were used. This number of sample points is much less than that of iteration in the initial registration and efficient for computational time. Various sample patterns were tested, including the case in which the sampling area has a bias for a true extremum. Curve fitting was also performed with a distance of 500, 650, or 850 mm between the X-ray focus and the femoral component.

Fig. 6 shows the absolute distance between the extremum of each polynomial and actual depth position, and its standard deviation. From these results, for fourth- and higher-order polynomials, the extremum error is almost saturated (about 0.5 mm), and also the tendency did not change even when the distance between the X-ray focus and the model changed. Thus, we used four for the order of the polynomial.

B. Accuracy Tests and Results

1) Computer Simulation Tests: Computer simulation tests were conducted to assess the improvement in depth position using the proposed technique. CAD models of femoral and tibial components (Dual Bearing Knee prosthesis: F3L and T3, Finsbury Development Ltd., U.K.) were rendered in known typical orientations using the perspective projection model. A set of ten synthetic contour images was then created for each component, without the addition of any artificial distortion or noise. Initial guess poses of the model were randomly chosen from within ± 10 mm and $\pm 10°$ of the correct values. Estimated poses are denoted by three translations and three rotations with respect to the X-ray focus. Errors in the 3-D pose of the model can then be determined by comparing the final estimated pose to the known pose.

For comparison of the proposed technique with other optimization techniques, the conventional technique using the Levenberg–Marquardt method (see Section II-D1) and the downhill Simplex method [20] modified by the simulated annealing (SA) algorithm [21] were demonstrated. In the SA algorithm, beginning with a seed arrangement at step k (the current pose), a transition is generated (step $\mathrm{k}+1$). The probability $\mathrm{P}(\Delta\mathrm{E})$ of accepting the transition depends on the difference $\Delta\mathrm{E} = \mathrm{E}(\mathrm{k}+1) - \mathrm{E}(\mathrm{k})$. For a transition resulting in a lower value of the cost function $(\Delta\mathrm{E} < 0)$, the new distribution is always accepted as the current one. Results showing an increase of the cost function $(\Delta\mathrm{E} > 0)$ are accepted with a probability given by $\mathrm{P}(\Delta\mathrm{E}) = \exp[-\Delta\mathrm{E}/\mathrm{T}(\mathrm{k})]$. Thus, for positive $\Delta\mathrm{E}$, transitions are accepted more easily at higher temperatures. The virtual temperature $\mathrm{T}(\mathrm{k})$ is generally scheduled in order to escape the local minimum. In our cooling schedule, $\mathrm{T}(\mathrm{k})$ was decreased by multiplying the current temperature by 0.9 for each iteration.

For efficient experimental tests, a visualization software system was developed. The system was implemented using the visualization tool kit [22], with all programs written in Visual C++, and was run on an Intel Pentium III computer, 1.2 GHz, 512 Mb RAM, under the Windows XP Professional edition.

The results of the computer simulation tests are summarized in Table I. The average errors of the two components are given, together with the standard deviation (SD) of the errors. The last three columns give the average RMSD, number of iterations and computation time. Table II also shows the root-mean-square errors (RMSEs).

The average errors of the five free variables, with the exception of Z axis translation, were not significantly different from zero, with average biases of approximately ± 0.1 mm and $\pm 0.1°$. The SD of the errors was found to be approximately 0.1 mm averaged over x and y translations, and approximately 0.2° averaged over the three rotations. Average errors in depth position increased from approximately -0.1 mm to -0.5 mm in comparison with the conventional optimization technique by applying the proposed technique, with the SD of the errors found to decrease from about 2.6 mm to 0.7 mm. In addition, RMSEs in depth position improved from about 2.6 mm to 0.9 mm for both components.

In the downhill Simplex method modified by SA, errors of depth position were found to be the same as or slightly better than the Levenberg–Marquardt method (conventional technique), while the computation time greatly increased. Thus, the conventional and proposed techniques based on the Levenberg–Marquardt method are highly efficient for computation time in the application of the contour-based registration described.

2) In Vitro Tests: In vitro tests were also performed by determining the absolute position and orientation of each component in order to assess improved depth position. Femoral and tibial components (Dual Bearing Knee prosthesis: F3L and T3, Finsbury Development Ltd., U.K.) were installed in artificial bones and the two components were linked by a string simulating the ligament between the femur and tibia. The 3-D poses

TABLE I
AVERAGE ESTIMATION ERRORS FOR COMPUTER SIMULATION TESTS OF TWO PROSTHESIS COMPONENTS (10 VIEWS FOR EACH COMPONENT). TRANSLATIONS AND ROTATIONS ARE REPORTED FOR OPTIMIZATION TECHNIQUES USING THE PROPOSED TECHNIQUE, THE CONVENTIONAL (LEVENBERG–MARQUARDT) TECHNIQUE, AND THE DOWNHILL SIMPLEX METHOD WITH SA. THE LAST THREE COLUMNS REPORT THE AVERAGE RMSD, THE NUMBER OF ITERATIONS (Ni), AND THE COMPUTATION TIME IN SECONDS (TIME)

Optimization techniques	Component	Average errors ± standard deviation for computer simulation tests						RMSD (mm)	Ni	Time (s)
		Translation (mm)			Rotation (degrees)					
		X	*Y*	*Z*	*X*	*Y*	*Z*			
Proposed	Femoral	0.031±0.034	-0.008±0.142	-0.518±0.761	-0.015±0.041	0.033±0.095	0.016±0.186	0.077	20	27
	Tibial	0.003±0.021	-0.014±0.141	-0.384±0.645	0.019±0.037	0.060±0.278	0.032±0.086	0.076	20	28
Conventional (Levenberg-Marquardt)	Femoral	0.017±0.088	-0.019±0.143	-0.120±2.510	-0.018±0.068	0.067±0.086	0.027±0.225	0.091	15	16
	Tibial	-0.005±0.047	-0.038±0.148	-0.112±2.665	0.033±0.041	0.040±0.310	0.037±0.080	0.086	16	16
Other (downhill Simplex + SA)	Femoral	0.002±0.088	-0.020±0.156	-0.155±2.225	-0.002±0.050	0.066±0.074	0.015±0.214	0.089	149	1311
	Tibial	-0.013±0.048	-0.022±0.151	-0.172±2.109	-0.009±0.033	0.060±0.258	0.016±0.064	0.081	179	1467

TABLE II
ROOT-MEAN-SQUARE ERRORS FOR COMPUTER SIMULATION TESTS OF TWO PROSTHESIS COMPONENTS. TRANSLATIONS AND ROTATIONS ARE REPORTED FOR OPTIMIZATION TECHNIQUES USING THE PROPOSED TECHNIQUE, THE CONVENTIONAL (LEVENBERG–MARQUARDT) TECHNIQUE, AND THE DOWNHILL SIMPLEX METHOD WITH SA

Optimization techniques	Component	Root-Mean-Square errors for computer simulation tests					
		Translation (mm)			Rotation (degrees)		
		X	*Y*	*Z*	*X*	*Y*	*Z*
Proposed	Femoral	0.048	0.161	0.934	0.044	0.110	0.187
	Tibial	0.022	0.153	0.755	0.043	0.245	0.097
Conventional (Levenberg-Marquardt)	Femoral	0.090	0.162	2.514	0.071	0.116	0.227
	Tibial	0.047	0.152	2.667	0.053	0.257	0.092
Other (downhill Simplex + SA)	Femoral	0.088	0.162	2.236	0.050	0.103	0.215
	Tibial	0.050	0.157	2.117	0.035	0.266	0.071

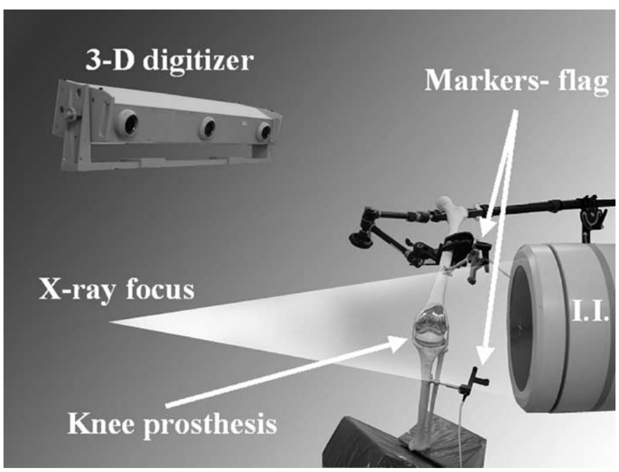

Fig. 7. Overview of *in vitro* experiment.

of each component could then be changed arbitrarily to emulate human knee motion. Fluoroscopic images were acquired for typical poses during standard dynamic motions. Images obtained in this manner differ from synthetic images due to image distortions, existing artificial bones, contour overlapping, X-ray scattering, etc.

A 3-D digitizer (Optotrak 3020: Northan Digital Inc, Canada) was used to determine poses for comparison with the estimations (Fig. 7). The digitizer is able to localize the 3-D positions of infrared LED markers and attached rigid body flag (markers-flag) with an accuracy of about 0.1 mm. First, a calibration board with markers-flag attached was measured using the digitizer. Following this, extrinsic parameters in the fluoroscopic system were determined by the calibration techniques described in Section II-B. Extrinsic parameters represent the transformation from the coordinate system of the X-ray fluoroscopy to that of the 3-D digitizer. Next, the two components that were installed in artificial bones were arranged in the viewing area. Fluoroscopic images were acquired at the same time, with two markers-flags fixed in the artificial femoral and tibial bones measured in each pose. To determine the relationship between the positions of each component and the corresponding markers-flag, 3-D points on the knee prosthesis surface were digitized in the markers-flag coordinate system, and surface registration of the 3-D points and knee implant CAD model was performed. The transformation from the fluoroscope coordinate system to the prosthesis coordinate system is then given by

$$
\begin{aligned}
&{}^{\mathrm{fluoroscope}}\boldsymbol{A}_{\mathrm{prosthesis}} \\
&\quad = \left({}^{\mathrm{3\text{-}D\ digitizer}}\boldsymbol{A}_{\mathrm{fluoroscope}}\right)^{-1} \cdot {}^{\mathrm{3\text{-}D\ digitizer}}\boldsymbol{A}_{\mathrm{flag}} \\
&\quad \cdot {}^{\mathrm{flag}}\boldsymbol{A}_{\mathrm{prosthesis}}
\end{aligned}
\tag{5}
$$

where each ${}^{x}\boldsymbol{A}_{y}$ is a 4×4 homogeneous transformation matrix of y with respect to reference coordinate system x. ${}^{\mathrm{fluoroscope}}\boldsymbol{A}_{\mathrm{prosthesis}}$ represent poses for comparison with the estimations.

Fluoroscopic images of the knee implants were taken in ten different poses with respect to the X-ray focus. For each image acquired, an initial guess pose for the estimation process was manually adjusted to be as close as possible. Experimental accuracy was assessed by comparing the final estimated pose with

TABLE III
AVERAGE ESTIMATION ERRORS FOR *IN VITRO* TESTS OF TWO PROSTHESIS COMPONENTS (10 VIEWS FOR EACH COMPONENT). TRANSLATIONS AND ROTATIONS ARE REPORTED FOR THE CONVENTIONAL (SECTION II-D1) TECHNIQUE AND THE PROPOSED TECHNIQUE. LAST COLUMN REPORTS THE AVERAGE RMSD

	Component	Average errors ± standard deviation for *in vitro* tests						RMSD (mm)
		Translation (mm)			Rotation (degrees)			
		X	*Y*	*Z*	*X*	*Y*	*Z*	
Conventional	Femoral	0.015±0.204	0.001±0.043	0.029±3.154	0.037±0.100	-0.028±0.138	0.051±0.644	0.285
	Tibial	-0.063±0.164	-0.090±0.169	-0.229±3.271	0.107±0.158	-0.174±0.713	0.039±0.090	0.197
Proposed	Femoral	-0.077±0.083	-0.020±0.020	-0.947±1.036	0.017±0.119	-0.012±0.125	0.070±0.633	0.274
	Tibial	-0.050±0.092	0.058±0.116	-0.901±0.989	0.070±0.169	-0.216±0.704	0.044±0.092	0.188

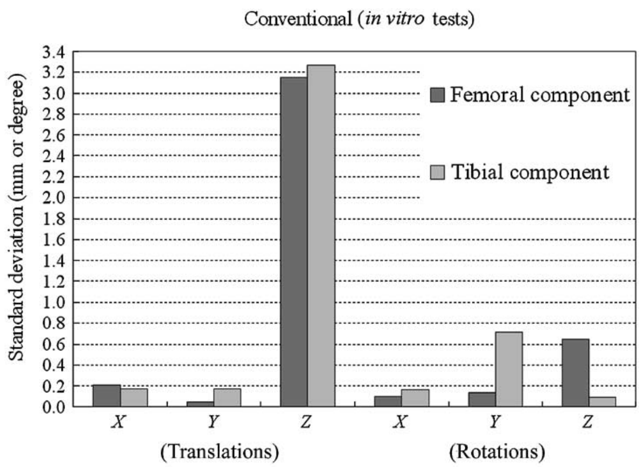

(a)

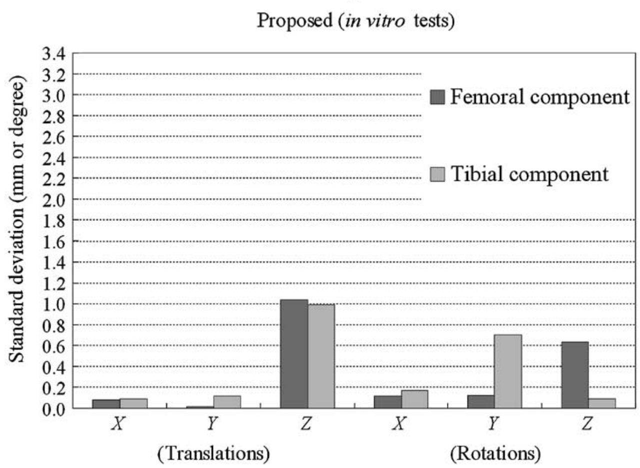

(b)

Fig. 8. Standard deviation of errors of the two prosthesis components for each variable (*in vitro* tests). (a) Conventional (Section II-D1) and (b) proposed techniques.

the pose determined by the 3-D digitizer. Errors in the conventional technique were also determined for comparison with the proposed technique.

The results of *in vitro* tests are summarized in Table III, in which the average errors of the two components, SD of the errors and average RMSD are listed. Fig. 8 shows the SD of errors of each variable for the two components before and after application of the proposed technique. Comparisons of RMSEs of the proposed technique with the conventional technique are given in Table IV. Fig. 9(a) and (b) shows a representative X-ray fluoroscopic image and an image of the CAD models overlaid with an X-ray image. Poses in the anteroposterior view showing poses of the models before and after application of the proposed technique, and the pose measured by the 3-D digitizer are shown in Fig. 9(c), (d), and (e), to demonstrate the effect of improved depth position.

Average errors of the five free variables except for Z axis translation were within ± 0.1 mm and $\pm 0.2°$, with the SD of the errors found to be about 0.1 mm averaged over the x and y translations and about 0.3° averaged over the three rotations. The average errors in depth position increased from about -0.1 mm to -0.9 mm by applying the proposed technique, with SD of the errors decreasing from about 3.2 mm to 1.0 mm. The RMSEs thus improved from about 3.2 mm to 1.4 mm. In addition, the improved depth position has been confirmed to be highly effective for demonstrating poses from the anteroposterior view.

3) In Vivo Tests: The consistency of the two components kept in constant relative position was validated in order to assess improved depth position because it is difficult to obtain accurate reference data for comparison with the estimates under *in vivo* conditions. A TKA patient was asked to stand straight in a state of maximum extension and not to move, with the knee relaxed as much as possible. Five different medio-lateral fluoroscopic images were then obtained by multidirectional radiography (taken at angles of approximately $\pm 15°$ and $\pm 30°$ when overlap of images at the medio-lateral condyle is defined as 0°). The consistency of the two components was demonstrated by determining the SD of errors for five estimated relative poses. The relative pose between the two components having the axis defined in Fig. 1(b) was determined by employing a three-axis Euler-angle system [23].

Table V gives the SD of errors for the conventional and proposed techniques. The direction of T_z in the relative pose is nearly aligned with the Z axis in the fluoroscope coordinate system. The SD of errors improved from about 4.9 mm to 1.5 mm by applying the proposed technique. The SD of errors for the other five free variables (T_x and T_y translations and three rotations) was also found to improve slightly.

Finally, we performed kinematic analysis of the full 6 DOF during dynamic motion of a TKA patient using the single-plane fluoroscopy-based system together with the proposed technique. A sequence of 29 images taken during rising from a chair was collected at 7.5 frame/s. For collected images, the initial guess pose used in the first frame was adjusted manually, but initial poses for subsequent frames were taken from the poses determined in the previous frame. The relative pose values (femoral component with respect to tibial component) are shown for each frame in Fig. 10.

TABLE IV
ROOT-MEAN-SQUARE ERRORS FOR *IN VITRO* TESTS OF THE TWO PROSTHESIS COMPONENTS. TRANSLATIONS AND ROTATIONS ARE REPORTED FOR THE CONVENTIONAL (SECTION II-D1) TECHNIQUE AND THE PROPOSED TECHNIQUE

	Component	Root-Mean-Square errors for *in vitro* tests					
		Translation (mm)			Rotation (degrees)		
		X	Y	Z	X	Y	Z
Conventional	Femoral	0.204	0.043	3.154	0.108	0.142	0.647
	Tibial	0.178	0.197	3.281	0.207	0.756	0.108
Proposed	Femoral	0.118	0.030	1.478	0.121	0.125	0.637
	Tibial	0.114	0.142	1.412	0.202	0.764	0.112

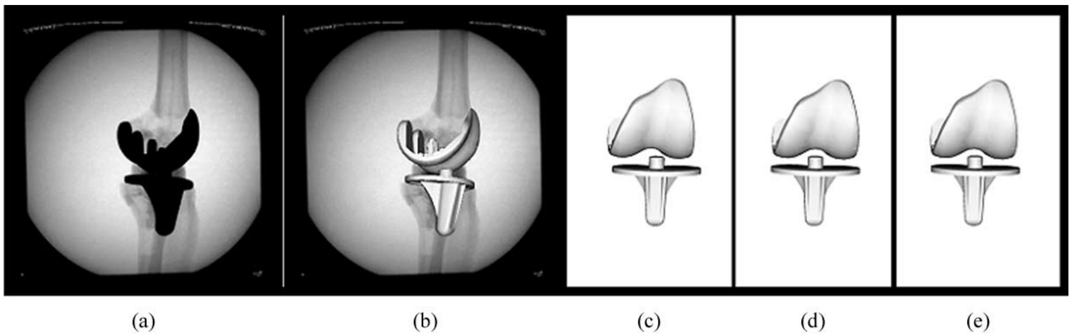

Fig. 9. Images from *in vitro* tests. (a) A representative X-ray fluoroscopic image (lateral view). (b) Image with CAD model overlay after pose estimation (proposed technique). (c)–(e) 3-D poses from the anteroposterior view. (c) Pose by the conventional technique (Section II-D1). (d). Pose by the proposed technique. (e) Pose measured by a 3-D digitizer. Improved depth position is observed in (d).

TABLE V
STANDARD DEVIATION OF ERRORS FOR *IN VIVO* TESTS OF RELATIVE POSES BETWEEN THE TWO COMPONENTS. THE RELATIVE POSES WERE MAINTAINED AT THE MAXIMUM EXTENSION AND ERECT POSITIONS, AND FIVE DIFFERENT MEDIO-LATERAL FLUOROSCOPIC IMAGES WERE USED. THE T_z DIRECTION IS APPROXIMATELY EQUAL TO THE Z AXIS DIRECTION IN THE FLUOROSCOPE COORDINATE SYSTEM

	Standard deviation for *in vivo* tests					
	Translation (mm)			Rotation (degrees)		
	T_x	T_y	T_z	θ_x	θ_y	θ_z
Conventional	0.564	0.557	4.931	0.783	1.106	0.317
Proposed	0.222	0.374	1.474	0.700	0.893	0.286

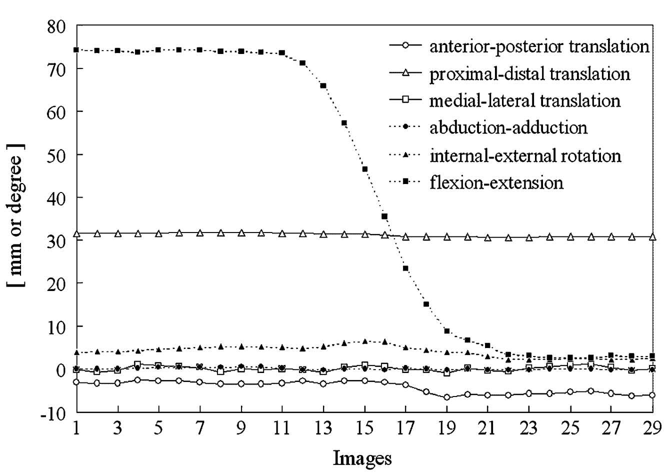

Fig. 10. Relative pose values of the knee prosthesis in a TKA patient during rising from a chair. Full 6 DOF (anterior-posterior, proximal-distal, and medial-lateral translations and abduction-adduction, internal-external rotation, and flexion-extension) are estimated from the 29 images analyzed.

IV. DISCUSSION

In this paper, we have presented a technique to improve the accuracy of the depth position of knee implants in 2-D/3-D registration using single-plane fluoroscopy, and suggested the possibility of full 6 DOF kinematic analysis. The present technique is based on the concept that accuracy of depth position is improved by optimizing it independently of the other 5 DOF. We quantified the behavior of the errors for each variable as evaluation curves. Results of preliminary experiments showed that when compared to the evaluation curves for the other 5 DOF, the evaluation curve for depth position was more jagged and the curve peak less pointy (see Fig. 4). In addition, the gradient of the curve changed markedly with distance between X-ray focus and the model [see Fig. 5(c)], and the scale for depth position was found to change continuously within and among evaluation curves. This suggests that, when all variables are optimized simultaneously, it is difficult to find an appropriate scale for depth position. However, the proposed technique does not require adjustment of the optimal scale as it employs an approximate evaluation curve, where a fourth-order polynomial is used.

In computer simulation tests, the accuracy of Z axis translation (depth position) improved drastically upon application of the proposed technique in terms of SD of error and RMSE (see Tables I and II). On the other hand, after the technique was applied, the average (bias) error of depth position for both components was approximately -0.5 mm. The cause for this may have been that the extremum (global minimum) of the evaluation curve for depth position deviated slightly from the correct value. Thus, even though a stable global minimum is obtained, a bias error occurs in the degree of this deviation. This bias error is thought to be caused by slight errors in translation parallel to fluoroscopic images. In order to reduce these slight errors, the contour of a projected image should be extracted at the subpixel level. However, the images that we used were high-resolution images (approximately 0.3×0.3 mm pixel size at 1024×1024 resolution, and 12×12 in II). Besides, contour extraction at the subpixel level would have been very time consuming and impractical. Hence, as in previous studies, contour extraction was carried out at the pixel level. For comparison to the downhill Simplex method [20] modified by SA [21], which can process cost function with arbitrary boundary conditions with a statistical guarantee of finding an optimal solution, accuracy of the depth position was only slightly better than that of the conventional technique based on the Levenberg–Marquardt method [18]. In the optimization by SA, there are generally problems such as adjustment of the virtual temperature and its cooling schedule, and the parameters were determined empirically in our study. Although the optimization was thought to be able to avoid the local minimum better than the conventional technique, it was not found to be effective with regard to computation time. Thus, an independent optimization based on the Levenberg–Marquardt method was presented. Consequently, the RMSE for depth position was about 2.6 mm with the conventional technique and about 0.9 mm with the proposed technique, thus suggesting that the obtained stable global minimum and decreased SD of error markedly improved the accuracy of depth position. The accuracy of the other 5 DOF with the proposed technique was almost the same as that achieved using the conventional technique.

In vitro tests were performed by determining the absolute position and orientation of each knee implant from the X-ray focus, which has not been investigated in previous studies. Thus, as with the computer simulation tests, we were able to verify the effects of improved accuracy of depth position. Through the use of the proposed technique, the accuracy of depth position improved drastically in terms of SD of error and RMSE (see Fig. 8, Table IV). As shown in Fig. 9(c), (d), and (e), the effects were also clear when both models were visualized from the anteroposterior direction. The slight differences in average bias, SD of error and RMSE observed between computer simulation and *in vitro* tests can be attributed not only to the inaccuracies in contour extraction caused by image noise and geometrical differences between CAD models and actual knee implants, but also to any errors in the 3-D digitizer (Optotrak) measurements. In this study, however, such measurement errors were not thoroughly investigated.

Image noise can be reduced by employing proper imaging techniques and giving an appropriate X-ray dose. As far as data acquisition and recording are concerned, we did not obtain image data by recording to videotape, but directly acquired high-quality serial digital images. Therefore, compared to normal videofluoroscopy, we were able to obtain fluoroscopic images with better contrast between the knee implant and the background.

The geometrical differences between a CAD model and an actual knee implant are an unavoidable problem when discussing accuracy of *in vitro* tests, and this issue has been investigated in previous reports [24]. The dimensions of the knee implant that we used were approximately $70 \times 70 \times 70$ mm, and its CAD model consisted of about 5000 triangle patches. The maximum error between the implant model and the CAD model was approximately 0.5 mm, and as a result, the errors may have reduced the accuracy of *in vitro* tests. However, this problem might be resolved as artificial joint manufacturing technology improves. Despite these known errors, we are very satisfied with the improved accuracy of depth position and other accuracy-related findings (see Table IV).

In our *in vivo* tests, utilizing the images of the lateral and oblique views at the maximum extension and erect positions of a patient, we verified the effects of improved depth position (medio-lateral direction). Because the knee joint is most stable in this pose and its movements are fixed, relative displacement of two implants caused by tension can largely be ignored. The SD of error for medio-lateral translation (T_z) improved markedly, and the SD of error for the other 5 DOF also improved slightly (see Table V). Although the tests were validated by the consistency of the relative pose, because it is difficult to obtain accurate reference data for comparison with the estimates, these results suggest the possibility of performing full 6 DOF kinematic analysis under *in vivo* conditions.

We also applied the proposed technique to *in vivo* kinematic analysis. Unlike previous studies, the knee kinematic analysis was carried out without fixing the medio-lateral translation between the two components at zero. As for the medio-lateral shift, the degree of change was much less than we expected (Fig. 10). The reason for this might have been that the implants were positioned properly by an orthopedic surgeon and their movements were stable. By examining the full 6 DOF, including medio-lateral shift, our system could have better detected and quantified abnormalities.

In our system, in order to obtain direct high-quality images, fluoroscopic images were acquired by serial shots of 7.5 frames/s, which was lower than in conventional video-fluoroscopy (30 frames/s). Although the frame rate was lower, as shown in Fig. 10, measurement values for all knee implants were smooth. Therefore, the present frame rate was sufficient for carrying out kinematic analysis of TKA implants.

In all of our experiments, the proposed technique was confirmed to sufficiently converge to the global minimum by executing conventional registration once again as described in Section II-D2). The amount of change in the 5 DOF, i.e., all except for depth position, was very small (see Tables I, II, III, and IV). Thus, we conclude that the solution obtained by the proposed technique is stable.

The proposed technique is a modified version of the technique of Zuffi *et al.* [6], but uses a higher resolution image and distance map. In addition to resolution, which they suggested, the estimated accuracy of their model tends to depend on the initial guess pose, but our study did not thoroughly investigate this problem. With some silhouettes prone to symmetric errors, a large initial guess error sometimes leads to a false pose. However, our visualization software system enabled inspection of the model from different directions and easy correction of its position. For the first frame, it was necessary to carefully adjust the initial guess pose. For subsequent frames, the final estimated pose of the previous frame was used as the initial guess pose.

In *in vitro* tests, by combining the improved global resolution and the depth position improvement technique, we were able to obtain accuracy for depth position of within 1.5 mm. On the other hand, in *in vivo* tests, the consistency obtained was about 1.5 mm. Although we are satisfied with these findings as far as improvement of depth position is concerned, full 6 DOF kinematics analyses, particularly depth analysis in clinical cases, requires further investigation.

ACKNOWLEDGMENT

The authors would like to thank Finsbury Orthopaedics Ltd. (Surrey, U.K.) and MMT Co. Ltd. (Osaka, Japan) for providing the computer model for the prosthesis components.

REFERENCES

[1] S. A. Banks, G. D. Markovich, and W. A. Hodge, "*In-vivo* kinematics of cruciate-retaining and -substituting knee arthroplasties," *J. Arthroplasty*, vol. 12, no. 3, pp. 297–304, 1997.

[2] W. A. Hoff, R. D. Komistek, and D. A. Dennis, "Three-dimensional determination of femoral-tibial contact position under *in-vivo* conditions using fluoroscopy," *Clin. Biomech.*, vol. 13, pp. 455–472, 1998.

[3] S. A. Banks and W. A. Hodge, "Accurate measurement of three-dimensional knee replacement kinematics using single-plane fluoroscopy," *IEEE Trans. Biomed. Eng.*, vol. 43, pp. 638–649, June 1996.

[4] W. A. Hoff *et al.*, "Pose estimation of artificial knee implants in fluoroscopy images using a template matching technique," in *Proc. 3rd IEEE Workshop Applications Computer Vision*, Sarasota, FL, Dec. 2–4, 1996, pp. 181–186.

[5] M. E. Sarojak, W. A. Hoff, R. D. Komistek, and D. A. Dennis, "Utilization of an automated model fitting process to determine kinematics of TKA," presented at the 23rd Annu. Meeting Amer. Soc. Biomech., Pittsburgh, PA, Oct. 1999.

[6] S. Zuffi, A. Leardini, F. Catani, S. Fantozzi, and A. Cappello, "A model-based method for the reconstruction of total knee replacement kinematics," *IEEE Trans. Med. Imag.*, vol. 18, pp. 981–991, Oct. 1999.

[7] S. Lavallee, J. Troccaz, P. Sautot, B. Mazier, P. Cinquin, P. Merloz, and J.-P. Chirossel, "Computer-assisted spinal surgery using anatomy-based registration," in *Computer-Integrated Surgery*, R. H. Taylor, S. Lavall'ee, G. C. Burdea, and R. Mosges, Eds. Cambridge, MA: MIT Press, 1996, pp. 425–449.

[8] J. Weese, G. P. Penney, P. Desmedt, T. J. Buzug, D. L. G. Hill, and D. J. Hawkes, "Voxel-based 2-D/3-D registration of fluoroscopy images and CT scans for image-guided surgery," *IEEE Trans. Inform. Technol. Biomed.*, vol. 1, pp. 248–293, Dec. 1997.

[9] G. P. Penney, J. Weese, J. A. Little, P. Desmedt, D. L. G. Hill, and D. J. Hawkes, "A comparison of similarity measures for use in 2-D-3-D medical image registration," *IEEE Trans. Med. Imag.*, vol. 17, pp. 586–595, Aug. 1998.

[10] J. B. Stiehl, R. D. Komistek, B. Hass, and D. A. Dennis, "Frontal plane kinematics after mobile bearing total knee arthroplasty," *Clin. Orthop.*, no. 392, pp. 56–61, 2001.

[11] B. M. You, P. Siy, W. Anderst, and S. Tashman, "*In vivo* measurement of 3-D skeletal kinematics from sequences of biplane radiographs: Application to knee kinematics," *IEEE Trans. Med. Imag.*, vol. 20, pp. 514–525, June 2001.

[12] H. Haneishi, Y. Yagihashi, and Y. Miyake, "A new method for distortion correction of electronic endoscope images," *IEEE Trans. Med. Imag.*, vol. 14, pp. 548–555, Sept. 1995.

[13] J. Weng, P. Cohen, and M. Herniou, "Camera calibration with distortion models and accuracy evaluation," *IEEE Trans. Pattern Anal. Machine Intell.*, vol. 14, pp. 965–980, Oct. 1992.

[14] J. Canny, "A computational approach to edge detection," *IEEE Trans. Pattern Anal. Machine Intell.*, vol. 8, pp. 679–698, Nov. 1986.

[15] J. S. Lim, *Two-Dimensional Signal and Image Processing*. Englewood Cliffs, NJ: Prentice-Hall, 1990.

[16] S. Lavallee and R. Szeliski, "Recovering the position and orientation of free-form objects from image contours using 3D distance maps," *IEEE Trans. Pattern Anal. Machine Intell.*, vol. 17, pp. 378–390, Apr. 1995.

[17] D. Kozinska, O. J. Tretiak, J. Nissanov, and C. Ozturk, "Multidimensional alignment using the Euclidean distance transform," *Graphic. Models Image Processing*, vol. 59, no. 6, pp. 373–387, 1997.

[18] D. G. Luenberger, *Linear and Nonlinear Programming*. Reading, MA: Addison Wesley, 1984.

[19] I. O. Kerner, "Ein gesamtschrittverfahren zur berechnung der nullstellen von polynomen," *Numer. Math.*, vol. 8, pp. 290–294, 1966.

[20] J. A. Nelder and R. Mead, "A simplex method for function minimization," *Comput. J.*, vol. 7, pp. 308–313, 1965.

[21] S. Kirkpatrick, C. D. Gelatt Jr., and M. P. Vecchi, "Optimization by simulated annealing," *Science*, vol. 220, pp. 671–680, 1983.

[22] W. Schroeder, K. Martin, and B. Lorensen, *The Visualization Toolkit: An Object-Oriented Approach to 3-D Graphics*. Englewood Cliffs, NJ: Prentice-Hall, 1996.

[23] E. S. Grood and W. J. Suntay, "A joint coordinate system for the clinical description of three-dimensional motions: Application to the knee," in *ASME J. Biomech. Eng.*, vol. 15, 1983, pp. 136–144.

[24] E. R. Valstar, F. W. de Joing, H. A. Vrooman, P. M. Rozing, and J. H. C. Reiber, "Model-based roentgen stereophotogrammetry of orthopaedic implants," *J. Biomech.*, vol. 34, pp. 715–722, 2001.